

Lawrence Berkeley National Laboratory

Recent Work

Title

Microstructure and Magnetic Anisotropy of Ultrathin Co/Pt Multilayers Grown on GaAs {bar over III} by Molecular-Beam Epitaxy

Permalink

<https://escholarship.org/uc/item/8xr3x5d7>

Journal

Journal of Applied Physics, 72(12)

Authors

Cho, N.-H.

Krishnan, K.M.

Lucas, C.A.

et al.

Publication Date

1992-04-01



Lawrence Berkeley Laboratory

UNIVERSITY OF CALIFORNIA

Materials Sciences Division

Submitted to Journal of Applied Physics

Microstructure and Magnetic Anisotropy of Co/Pt Multilayers Grown on GaAs III by MBE

N.-H. Cho, K.M. Krishnan, C.A. Lucas, and R.F. Farrow

April 1992

For Reference

Not to be taken from this room



DISCLAIMER

This document was prepared as an account of work sponsored by the United States Government. While this document is believed to contain correct information, neither the United States Government nor any agency thereof, nor the Regents of the University of California, nor any of their employees, makes any warranty, express or implied, or assumes any legal responsibility for the accuracy, completeness, or usefulness of any information, apparatus, product, or process disclosed, or represents that its use would not infringe privately owned rights. Reference herein to any specific commercial product, process, or service by its trade name, trademark, manufacturer, or otherwise, does not necessarily constitute or imply its endorsement, recommendation, or favoring by the United States Government or any agency thereof, or the Regents of the University of California. The views and opinions of authors expressed herein do not necessarily state or reflect those of the United States Government or any agency thereof or the Regents of the University of California.

**Microstructure & Magnetic Anisotropy
of Co/Pt Multilayers Grown on GaAs (111) by MBE**

N.-H. Cho#, K.M. Krishnan*, C.A. Lucas** and R.F. Farrow†

*Materials Science Division
National Center for Electron Microscopy
Lawrence Berkeley Laboratory
University of California, Berkeley, CA 94720

#Korea Institute of Science & Technology
Fine Ceramics Laboratory, Seoul, Korea

** Center for Advanced Materials

†IBM Almaden Research Center
650 Harry Road, San Jose, CA 95120

Submitted to Applied Physics Letters

This work was supported in part by the Director, Office of Energy Research, Office of Basic Energy Sciences, Materials Science Division of the U.S. Department of Energy under Contract No. DE-AC03-76SF00098, and a postdoctoral research fellowship from IBM.

Microstructure and magnetic anisotropy of Co/Pt multilayers grown on
GaAs ($\bar{1}\bar{1}\bar{1}$) by MBE

N.-H. Cho*[#], Kannan M. Krishnan*^{\$}, C. A. Lucas**,

Materials Sciences Division,

Lawrence Berkeley Laboratory, Berkeley, CA 94720

and

R. F. C. Farrow

IBM Almaden Research Center

650 Harry Road, San Jose, CA 95120

* National Center for Electron Microscopy

** Center for Advanced Materials

Present address: Fine Ceramics Laboratory, Korea Institute of Science and Technology, Seoul, Korea.

\$ To whom all future correspondence should be addressed.

Abstract

Multilayers of $[\text{Co}_{3\text{Å}}, \text{Pt}_{15\text{Å}}]_x$, $x = 15$ or 30 repeats, with or without a 200Å silver buffer layer, were grown on GaAs ($\bar{1}\bar{1}\bar{1}$) substrates by molecular beam epitaxy (MBE). Vibrating sample magnetometry (VSM) measurements confirmed that the samples with the Ag buffer layer show strong uniaxial magnetic anisotropy perpendicular to the surface. The perpendicular anisotropy exhibited by these metallic superlattices is discussed in terms of the microstructure of the overall multilayer stack, as well as the structural characteristics of the Co interface layer.

Samples grown on the Ag buffer layer show strong (111) texture with 30-40nm size twin related grains. These grains, correspond to the two possible (111) stacking sequence for an fcc lattice, i.e. double positioning. However, direct growth on GaAs ($\bar{1}\bar{1}\bar{1}$) results in randomly oriented 10-20 nm grains.

All samples exhibit a repeat period of 1.83 nm in both low angle reflectivity and high angle $\Theta-2\Theta$ x-ray scattering measurements. In addition, transverse scans through the low angle multilayer Bragg peaks show the interfaces to be diffuse in nature indicative of considerable in-plane inhomogeneity and/or compound formation. High resolution electron microscopy measurements of cross-sections compared with image simulations confirm that the interface layer is diffuse and its stoichiometry is such that the Co occupation is less than 40%. Redistribution of Co should then extend over at least four monolayers.

The nanostructure comprises of an eight atomic layer repeat with the Co interface layer diffuse over a few monolayers. The microstructure is strongly (111) textured with columns of twin related 30 nm sized grains separated by a 1nm wide second phase. It is suggested that the combination of interdiffusion, highly oriented but twin related columnar growth, small grain size with a nanometer-scale second phase may be the key to the understanding of the perpendicular anisotropy observed in these (111) superlattices.

INTRODUCTION

There is significant interest in ultrathin metallic multilayers because of their novel magnetic properties and potential device applications. These properties include perpendicular magnetic anisotropy [1,2], giant magnetoresistance [3], antiferromagnetic coupling [4] and long range oscillatory coupling [5].

Various thin film growth techniques such as molecular beam epitaxy (MBE), sputtering, and evaporation have been used to produce these multilayer stacks. In particular, MBE growth [6] of these structures has the advantage of growing well oriented layers with high degree of crystallinity. This permits a critical evaluation of the dependence of the magnetic properties of the film on orientation, crystallography and microstructure. Semiconductor substrates are highly perfect in structure and with appropriate seeding one can control both the epitaxy and growth orientation in MBE deposition. Growth of magnetic thin films on semiconductor substrates is also of interest for potential device integration [7].

Perpendicular magnetic anisotropy has been observed in multilayers of Co or Fe sandwiched between non-magnetic metallic layers grown by MBE [2]. Apart from this unique but poorly understood magnetic behaviour, this property makes the Co/Pt multilayers attractive as a potential media for magneto-optical information storage. The anisotropy has generally been attributed to the broken-symmetry [8] at the interfaces between magnetic and non-magnetic metals as well as formation of a relevant alloy at the interfaces [9]. Structural defects such as planar defects [10] along the growth direction have also been discussed as sources for the strong anisotropy. However, in recent studies of MBE grown Co/Pt multilayers [11], magnetic properties are shown to be dependent on

the growth direction. Superlattices grown along the (111) axis exhibit perpendicular anisotropy with well defined square loops, while superlattices grown along the $\langle 100 \rangle$ axis exhibit in-plane anisotropy except for a Co thickness of 1 monolayer where a weak perpendicular anisotropy is detected [12]. The (110) oriented superlattices show intermediate behaviors. This suggests that perpendicular anisotropy in the multilayers cannot be explained by simple arguments of surface anisotropy and broken-symmetry at the interfaces, and a more detailed investigation of the crystallography and microstructure of the multilayers is required.

In order to understand the origin of the perpendicular magnetic anisotropy, we have been investigating the relationship between the microstructure and magnetic properties of these multilayers. In this paper, we present three different structures of Co/Pt multilayers: $[\text{Co}_{3\text{\AA}}, \text{Pt}_{15\text{\AA}}]_x$, $x = 15$ or 30 repeats, grown on GaAs $(\bar{1}\bar{1}\bar{1})$ by MBE with a 200Å thick Ag buffer layer. The latter sample ($x = 30$ repeats) was also grown without the Ag buffer layer. Magnetic anisotropy of these structures were examined using a VSM. These magnetic properties are discussed in terms of the microstructure of the multilayers as well as the structural characteristics of the interfaces. Twin formation in the multilayers and the epitaxial relationship between the various components of the multilayer stack were studied by transmission electron microscopy using both plan and cross-section view samples. In addition, these structural measurements were correlated with high angle x-ray scattering experiments. Structural characteristics at the interfaces, i.e. periodicity of the multilayers, and homogeneity of the interfaces, were investigated by low angle X-ray reflectivity and related transverse rocking scan experiments [13].

EXPERIMENTAL

1. Film growth

Thirty periods of $\sim 3 \text{ \AA}$ Co/ $\sim 15 \text{ \AA}$ Pt layers, without or with a 200 \AA thick Ag buffer layer, and fifteen periods of $\sim 3 \text{ \AA}$ Co/ $\sim 15 \text{ \AA}$ Pt layers, with the Ag buffer layer were grown on GaAs substrates by a VG 80-M MBE system. Figure 1 shows a schematic representation of these three different structures and are referred to as samples A, B, and C in this paper.

GaAs substrates were cut such that the surface normal was less than 0.5° from the exact [111] axis. Prior to loading the substrates into the system they were chemically etched as described earlier [11]. The substrates were heated to $\sim 600^\circ\text{C}$ in a background pressure of $< 10^{-10}$ mbar to remove surface impurities and to generate a 1×1 RHEED pattern. Ag layers were grown at a rate of $0.35 \text{ \AA}/\text{sec}$ from a Knudsen cell held at $\sim 1050^\circ\text{C}$. The Co and Pt layers were grown from e-gun sources at rates of 0.15 and $0.25 \text{ \AA}/\text{sec}$, respectively. The background pressure before and during the film growth was approximately 2×10^{-11} mbar.

2. Vibrating Sample Magnetometer

A commercial VSM was used to measure the magnetic properties (B-H loops) of the multilayers. All measurements were carried out at room temperature. The applied magnetic field strength range from -10 kOe to $+10 \text{ kOe}$. The sensitivity of the induced magnetization was 10^{-3} emu. The sample size was $\sim 5 \times 5 \text{ mm}^2$.

3. X-ray Scattering

X-ray scattering measurements were performed on a double-crystal diffractometer utilizing a 12 kW rotating anode x-ray generator with a copper target. $\text{Cu K}\alpha_1$ x-rays

($\lambda=1.541 \text{ \AA}$) were selected and collimated by reflection from a Ge (111) monochromator crystal followed by a slit to eliminate the Cu $K\alpha_2$ component. Each sample was oriented with its surface normal in the scattering plane and the scattered x-rays were detected by a scintillation counter after passing through a 0.5 mm slit. The scattering plane resolution of the instrument is determined by the incident beam profile and the detector slit width giving an angular resolution of FWHM $\sim 0.015^\circ$.

Measurements of low-angle reflectivity and high angle diffraction were carried out in the form of θ - 2θ scans. A θ - 2θ scan measures the scattered intensity as a function of wave-vector transfer along the sample surface normal in reciprocal space. Rocking scans through the reflectivity rod, i.e., perpendicular to the surface normal, were also performed to probe the in-plane structural perfection.

4. Transmission Electron Microscopy

High-resolution transmission electron micrographs were recorded using the Atomic Resolution Microscope (ARM) operating at 800 kV at the National Center for Electron Microscopy. Spherical aberration (Cs) and point to point resolution of the microscope were 2.3 mm and 1.7 \AA , respectively. Conventional TEM study of the multilayers was performed using a JEOL 200 CX microscope operating at 200 kV.

Cross-section and plan view specimens for TEM were prepared by standard mechanical dimpling followed by ion beam milling [14].

RESULTS

1. Magnetic Property Measurements

Magnetic properties (B-H loop) measured from the three samples are shown in figure 2. The hysteresis loop from samples A, B, and C exhibit a squareness ratio (B_r/B_m : B_m is maximum magnetic induction, B_r : remanence) of 0.35, 0.97, and 0.66, respectively. Coercivity of samples A, B, and C are 1.1×10^3 Oe, 3.7×10^3 Oe, and 3.7×10^3 Oe, respectively.

2. X-ray Scattering Experiments

Low angle reflectivity measurements in the form of θ - 2θ scans are shown for all three samples in figure 3. No background subtraction of the data has been attempted. The first and second order satellites are clearly resolved and enable a repeat period in the multilayer structures to be calculated. This calculation corrects for the effects of refraction. The calculated d-spacing of the multilayer is 18.4 \AA .

Rocking scans, representative of all three samples, are shown for sample B in figure 4. The figure shows transverse rocking scans at two values of scattering angle 2θ , (a) at 2.0° (b) at the position of the first order multilayer satellite, 4.9° . In (a) although there is considerable scattering away from the specular peak it is still possible to observe a resolution-limited specular peak characteristic of long range order in the sample surface plane. In (b) the scattering is entirely diffuse with no observable specular peak.

High angle scattering curves for sample A (figure 5) and for samples B and C are shown in figure 6. These figures show that there is considerable difference between sample A, the sample with no silver buffer layer, and the other two samples (B and C). The most intense peak at $2\theta=40.6^\circ$ is the zero order peak of the superlattice. This is

accompanied by satellite reflections, labelled in figure 6, at $2\theta=30.5^\circ$, 35.5° and 45.6° . The spacing of these satellites can be related to the repeat period of the crystalline Pt in the structure, i.e., $\Delta Q = 2\pi/d$, the scattering vector $Q = (4\pi/d)\sin \theta$, which gives a spacing $d=18.3 \text{ \AA}$. This is in agreement with the low angle reflectivity data. The peak at $2\theta=38.2^\circ$ is due to the Ag (111) buffer layer. The peak at $2\theta=44.9^\circ$ is due to x-rays scattered from the sample holder. No clear evidence of any scattering due to crystalline Co is observed, although there does appear to be a weak feature at $2\theta=44^\circ$ in the data of sample B.

The data of figure 5 for sample A shows none of the observed features for the other two samples. There is a peak at $2\theta=40.6^\circ$ corresponding to a Pt (111) reflection but a rocking scan at this angle shows no peak at $\theta=1/2(2\theta)$ indicating that the platinum has a polycrystalline structure.

Table I shows a summary of peak positions and widths (as measured by rocking the crystal at the 2θ value, i.e. a θ scan) for the high angle diffraction data from all three samples. This is most instructive for samples B and C. The rocking curve widths are inversely related to crystalline quality. Samples B and C appear to have better crystalline quality than sample A. In general it is possible to simulate the observed scattering using a kinematical theory of x-ray diffraction [15,16]. However, to correctly obtain the observed intensities and widths a model of the structure including compositional mixing at the interfaces would be required and such analysis is not attempted here.

3. Transmission Electron Microscopy

Bright field images obtained from plan-view specimens of samples A and C are shown in figure 7a and figure 7c, respectively. These images were recorded from areas of the deposited films with electron beams nearly parallel to the (111) axis of the GaAs substrate. Deposited multilayers of samples A and C appear to be polycrystalline consisting of grains 10-20 nm, and 30-40 nm in diameter, respectively. The grain

boundaries are ~ 1 nm wide in both samples. The corresponding selected area diffraction patterns in figure 7b suggest that the films in sample A are composed of randomly oriented Pt grains. On the other hand, six-fold symmetry is observed in the SAD for sample C, figure 7d; this is unexpected from the bright field image seen in figure 7c. All spots in figure 7d show an angular spread less than 2° .

Figure 8 shows one of the high-resolution images from the plan-view specimens of sample C. This image was obtained with electron beams parallel to the (111) orientation. Lattice images corresponding to (111) planes in both grains M and N exhibit 3-fold symmetry, but a misorientation of $\sim 2^\circ$ about (111) axis is seen between the two grains. No crystalline phase is seen at the boundary between the two grains.

High resolution images obtained from cross section specimens of samples A and C are shown in figure 9a and 9b, respectively. These micrographs were recorded with electron beams parallel to [110] axis of GaAs substrate. Micrograph in figure 9a shows polycrystalline structure of the films deposited on GaAs substrate. On the otherhand, good epitaxial relationship between GaAs substrate and Ag buffer layer is observed; the {111} planes of the Ag layer are parallel to the {111} planes of the GaAs substrates.

Twin related grains, 30-40 nm in diameter, are present in all the components of the multilayer stack. These twins are generated either by the propagation of the twin boundaries in the Ag layer into the multilayers or by nucleation of twin-related Pt grains on the Ag buffer surface [17]. Rotational Moire fringes with three times the $(111)_{\text{Pt}}$ spacing along the growth direction, due to superposition of these twin related grains are observed in both the Ag buffer layer and the Co/Pt multilayer stack. Details of the contrast mechanism giving rise to such fringes are discussed elsewhere [17].

Arrows D and E indicate edge dislocation cores near the interface between the buffer layer and the Co/Pt multilayers. The Co/Pt multilayers are also observed to be in

good epitaxial relationship with the buffer layer. Individual components of the multilayer stack in the image, such as the Ag layer, Co/Pt superlattices and the GaAs substrate, was confirmed by matching the spatial frequencies obtained in optical diffractograms with known lattice spacings. {111} lattice planes of grains M and N indicate that one grain is related to the other by a rotation of 70.5° about the [110] axis.

4. X-ray Emission Spectroscopy

A representative XES from a plan view sample after the removal of the GaAs substrate is shown in figure 10. This was obtained from the area where the bright field image shown in figure 7 was recorded. Pt and Co are the main species and small amount of Ga, As and Ag, probably due to redeposition in the ion-milling process, are detected.

DISCUSSION

1. Nature of the Co interface layer

The structure of the Co layer and the nature of the Co/Pt interface is critical in interpreting the origin of perpendicular anisotropy in these films. For the three samples discussed in this paper, because the dimension of the Co component of the multilayer stack is of the order of a monolayer, the definition of the layer and its interface with the adjacent Pt layer is blurred. However, earlier studies [20] with $\langle 100 \rangle$ and $\langle 111 \rangle$ oriented multilayers, suggest that there is a sizable interdiffusion at the Co/Pt interface. This was interpreted to imply the presence of either an ordered CoPt_3 alloy phase [9] or substantial in-plane disorder such as interfacial roughness.

The position of the satellite reflections in the high angle diffraction data (Figures 5 & 6) correspond to a Pt crystalline phase in the samples with a repeat period $d=1.83$ nm. This is also in agreement with the calculated period from the positions of the satellites in the low angle reflectivity data, i.e. $d=1.84$ nm. However, transverse rocking scans through the low angle multilayer Bragg peaks from all three samples (Figure 4) show them to be diffuse in nature. Quantitative analysis of the measurements is difficult as the in-plane structure necessitates a three dimensional structural model of the Co layer in order to simulate the scattering. Such interpretation would be ambiguous without independent structural information. However, from these results initial conclusions are that the samples contain considerable in-plane inhomogeneity consistent with interfacial mixing and compound formation at the interface.

To further elucidate the structure of the Co interface layer, high resolution transmission electron micrographs of cross-section samples over a wide range of sample thickness and objective lens defocus values were obtained (Figure 11). Structural interpretation from such images requires careful matching of simulated and experimental images, preferably over a range of defocus and thickness values [21].

Image simulations using the NCEMSS [22] package for a number of different structural models of the Co interface layer were carried out. The probability of Co in the interface layer was varied in steps of 10% from 100% to 20% and this change in composition was accomplished by balancing the probability of Co occupation in the adjacent Pt layers. These models of the graded interface(s) are summarized in figure 12. Note that in the later structural model actual sites for the Co atoms are not defined but appropriate probabilities, in keeping with the atomic ratios, are assigned for the different layers. Results of the simulations for a uniform monolayer of Co, sandwiched between seven layers of Pt, are shown in figure 13a. In almost all the imaging conditions, for two

representative sample thicknesses, these simulation predict that the columns of atoms in the Co interface layer can be clearly resolved. However, if the interface composition is graded and the probability of Co occupation in the interface layer is less than 40%, it is clear from the simulations (figure 13b) that, inspite of the large difference in scattering factors for Co and Pt, high resolution electron micrographs will not resolve the interface layer.

Neither the contrast in high resolution micrographs obtained so far, nor the spatial frequencies in the optical diffractograms from the multilayer regions in the negatives, indicate such 1.83 nm periodicity. Based on our extensive simulation of images for a variety of structural models [19], we can conclude that the Co atoms are not present as a monolayer but are mixed with Pt such that its occupation in any given site is less than 40%.

In principle, these results are in agreement with the x-ray rocking scans, particularly the diffuse low angle reflectivity measurements. Further, *in-situ* x-ray photoelectron diffraction studies of the Co-Pt interfaces during their formation suggest that they are not atomically abrupt but are diffused over four monolayers [20]. This interpretation is also consistent with preliminary high resolution z-contrast images [23] of these multilayers that indicate a distribution of 6-8Å for the Co layers in these samples.

The structure of the Co interface layer is critical in understanding the origin of perpendicular anisotropy in these films. From the X-ray and HREM measurements the following conclusions can be drawn: (a) The Co interface layer is diffuse - evidence for atomic mixing and compound formation is present in both measurements; (b) the exact stoichiometry or the structure of the inerface layer is still unclear, given the wide range of miscibility for Co in Pt [18].

2. Microstructure of the Co/Pt multilayers

For the samples produced with a Ag layer as a buffer, the bright field image (figure 7c) indicate that the multilayers are polycrystalline with an average grain size of 30-40 nm. However, the corresponding selected area diffraction pattern (figure 7d) is that of a typical single crystal. This contradiction can be resolved by the following arguments. A rotation of 60° about the [111] axis results in two different stacking sequences for a face centered cubic lattice. These can be represented symbolically as ABCABC..., and BACBAC.... These sequences are twin related and give rise to identical selected area diffraction patterns for the incident electron beam parallel to the [111] axis. However, small angular deviation ($< 2^\circ$) from the exact twin-related orientations, along with the presence of a non-crystalline intergranular phase (~ 1 nm wide) distinguish one grain from the other clearly in the bright field images (figure 7c).

The presence of these twin grains are also well identified in the corresponding high resolution images. In general, the twin boundaries propagate across the length of the multilayer stacks, forming 30-40 nm size grains. The angular deviation along the [111] axis is considered to be $< 2^\circ$ from the parallel alignment of the {111} planes of the multilayers with the {111} planes of the GaAs substrates (Figure 9). Consequently, the multilayers grown with the Ag layer as a buffer consist of twin-related grains, which are well textured perpendicular to the substrate. In contrast, the high resolution images and selected area diffraction patterns obtained from cross-section and plan-view specimens of the multilayers grown without the Ag buffer layer confirms that these structures are polycrystalline and consist of 10-20 nm randomly oriented grains.

Peak widths, in the high angle x-ray rocking curve measurements, are inversely related to the crystalline quality. Narrow line widths for samples B and C indicate that multilayers of these samples have better crystalline quality than sample A. For samples B

and C, low angle misorientation ($\sim 3-4^\circ$) about the [111] axis, in addition to the strain field caused by lattice mismatch between the multilayers and the substrate (or the Ag layer), may cause rocking scan curve widths ($2-3^\circ$) to be larger than that (0.2°) of GaAs substrates.

It can be concluded that the deposition of a Ag buffer layer enhances the crystalline quality of the multilayers and also lead to better epitaxy between the multilayers and the substrates. In other words, the Ag buffer layer prevents the Co/Pt multilayer from growing in random orientations and promotes the deposition of the multilayers in a particular growth orientation, albeit twin related.

3. Magnetic anisotropy - structure relation

It is instructive to note that all the multilayer stacks (samples A, B, and C) have the same characteristics at the Co interface layer. Atomic mixing and/or compound formation at the interface is clearly evident. However, the presence of an ordered $L1_2$ phase of CoPt_3 , suggested earlier [9], is far from confirmed. Both experimental measurements [24] and calculations [18] suggest that the Curie temperature (T_C) for this alloy phase depends on the degree of chemical ordering in the alloy and can vary from 420K to 550K (at the exact 25-75% composition). T_C measurements of these multilayer stacks as a function of temperature should provide conclusive evidence about the existence of the ordered alloy phase. Deposition of the multilayers on substrates other than GaAs, such as sapphire, is required for such measurements. This work is in progress and will be discussed elsewhere.

The twin related grain growth results in a columnar texture in the Co/Pt multilayers. In addition, these 30-40 nm size grains are separated by a 1nm wide non-crystalline intergranular phase. In principle, this type of morphology could lead to a magnetically connected microstructure - the diffuse Co interface layers in the multilayer stack being coupled through the depth of the film by this second phase. The crystallography,

chemistry and magnetic properties (anisotropy constants etc) of this phase needs to be investigated in detail to create a more exact model. This kind of microstructural interpretation could also account for the difference in perpendicular anisotropy observed in films grown along various crystallographic orientations.

ACKNOWLEDGEMENT

We would like to thank Dr. C. H. Lee for MBE growth of Co/Pt multilayers, Dr. R. Kilaas for performing image simulation of high resolution transmission electron micrographs, Mr. C. Nelson for assistance in using the ARM at the National Center for Electron Microscopy, M. Chandramouli for help in VSM measurements, Mr. C. Echer for assistance in XES operation and Dr. Bing Zhang for helpful discussions. N.-H. Cho would like to acknowledge a postdoctoral research fellowship from IBM Almaden Research Center. This research was supported by the Director, Office of Energy Research, Office of Basic Energy Sciences under contract number DE-AC03-76SF00098.

REFERENCES

1. F.J.A. den Broeder, D. Kuiper, H.C. Donkersloot, and W. Hoving, *Appl. Phys.* **A49**, 507 (1989).
2. W.B. Zeper, F.J.A.M. Greidanus, P.F. Carcia, and C.R. Fincher, *J. Appl. Phys.*, **65**(12), 4971 (1989).
3. M.N. Baibich, J.M. Broto, A. Fert, F. Nguyen Van Dau, F. Petroff, P. Erienué, G. Creuzet, A. Friederich, J. Chazelas, *Phys. Rev. Lett.*, **61**, 2472 (1988).
4. F. Saurenbach, J. Barnas, G. Binasch, M. Vohl, P. Grunberg, W. Zinn, *Thin Solid Films*, **175**, 317 (1989).
5. S.S. Parkin, S. Fan, N. More, K.P. Roche, *Phys. Rev. Lett.* in press (1990).
6. R.F.C. Farrow, C.H. Lee, *Mat. Res. Soc. Symp. Proc.* **187**, 211 (1990).
7. G.A. Prinz, Paper presented at 119th Annual Meeting of the Metallurgical Society, Anaheim, Ca (1990).
8. P. Bruno, and J.-P. Renard, *Appl. Phys.*, **A49**, 499 (1989).
9. C.J. Chien, R.F.C. Farrow, C.H. Lee, C.J. Lin, and E.E. Marinero, *J. Magnetism and Mag. Mat.*, **93**, 47 (1991).
10. C.J. Lin, G.L. Gorman, C.H. Lee, R.F.C. Farrow, E.E. Marinero, H.V. Do, H. Notarys, C.J. Chien, *J. Magnetism Mag. Mat.*, **93**, 194 (1991).
11. C.H. Lee, R.F.C. Farrow, C.J. Lin and E.E. Marinero, C.J. Chien, *Physical Rev.*, **B42**(17), 11384 (1990).

12. D. Weller, R. F. C. Farrow, R. F. Marks, C.H. Lee and G. Harp, Phys. Rev B, to be submitted (1992).
13. D.E. Savage, J. Kleiner, N. Schimke, Y.H. Phang, T. Jankowski, T. Jacobs, R. Kariotis and M.G. Lagally, J. Appl. Phys., **69**, 1411 (1991).
14. J. C. Bravman and R. Sinclair, J. Elec. Microsc. Technique, **1**, 53 (1984)
15. R.M. Fleming, D.B. McWhan, A.C. Gossard, W. Wiegmann, and R.A. Logan, J. Appl. Phys., **51**, 357 (1980).
16. M. Quillec, L. Goldstein, G. LeRoux, J. Burgeat and J. Primot, J. Appl. Phys., **55**, 2904 (1984).
17. N.-H. Cho, K.M. Krishnan, C.H. Lee and R.F.C. Farrow, Appl. Phys. Lett., in press (1992).
18. J.M. Sanchez, J.L. Moran-Lopez, C. Leroux, and M.C. Cadeville, J. Physique, **C8** - 107 (1988).
19. N.-H. Cho, K.M. Krishnan and R. Kilaas, Ultramicroscopy, in preparation (1991).
20. B.D. Hermsmeier, R.F.C. Farrow, C.H. Lee, E.E. Marinero, C.J. Lin, R.F. Marks, and C.J. Chien, J. Appl. Phys., **69**(8), 5646 (1991).
21. T. Epicier, M. A. O'Keefe and G. Thomas, Acta Cryst., **A46**, 948 (1990)
22. NCEMSS, Public domain software distributed by the NCEM, LBL, Berkeley.
23. K. M. Krishnan, unpublished data.
24. C. Leroux, Ph. D. dissertation, L'Universite Louis Pasteur, Strassbourg (1989)

FIGURE CAPTIONS

Figure 1. Schematic representation of the multilayer structures; (a) sample A; (b) sample B; (c) sample C. Each multilayer is terminated with Pt layer, and a 75 Å thick amorphous Si₃N₄ layer is capped on the multilayers to prevent the films from oxidation.

Figure 2. Magnetic properties (B-H loops) of the multilayers: (a) sample A; (b) sample B; (c) sample C.

Figure 3. Low angle reflectivity data for the multilayers for a range of incident angle $\theta=0.8^\circ-5.2^\circ$. The data are displaced for clarity. Two satellite reflections are seen at $2\theta=2^\circ$ and 4.9° for samples A, B, and C. There is no data in the range $2\theta = 3^\circ - 4.5^\circ$. The two sets of data are connected by a straight line.

Figure 4. Transverse scans across the reflectivity rod (θ scans): (a) at $2\theta=2.0^\circ$; (b) $2\theta=4.9^\circ$. In (a) the spectrum shows a sharp specular peak at $\theta=1.0^\circ$. In (b) no sharp specular peak is observed, i.e., the scattering is entirely diffuse in nature.

Figure 5. High angle diffraction data (of sample A). The peak positions and widths, obtained from rocking scans, are shown in Table 1.

Figure 6. High angle diffraction data (of samples B and C). The data are displaced for clarity.

Figure 7. Bright field images and corresponding selected area diffraction patterns: (a) & (b) sample A; (c) & (d) sample C.

Figure 8. High resolution image from plan-view specimen of sample C. Three-fold symmetry in the individual grains, a non-crystalline second phase and a small misorientation between the grains can be seen.

Figure 9. High resolution images from cross-section view specimen of (a) sample A; (b) sample C. In (a) randomly oriented grains are observed in the multilayers. In (b) well textured twin-related grains with the [111] axis parallel to the substrate surface normal are seen in the multilayers.

Figure 10. X-ray emission spectrum from sample C

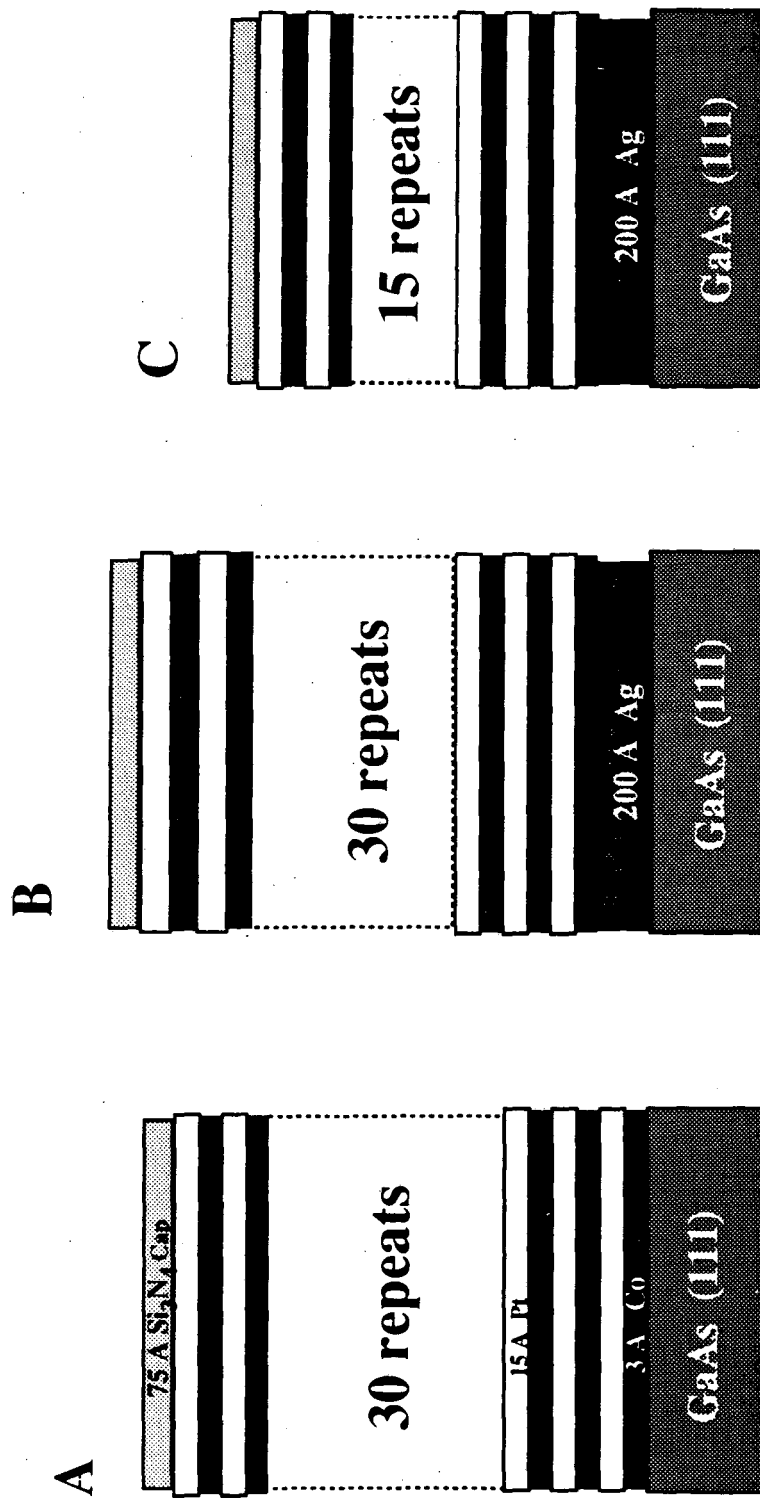
Figure 11. A representative area of the high resolution image without any overlapping grains.

Figure 12. Structural models of the interface layer used in image simulation. The probability of Co occupation in the interface layer was varied. In each case, the excess Co was redistributed in the adjacent Pt layers to give rise to a smoothly graded interface.

Figure 13. Results of the image simulation for a range of defocus (in 100Å steps) and two sample thicknesses. (a) Sharp interface monolayer with 100% Co occupancy and (b) graded interface with 40% Co at the interface layer - Note that the Co layer is barely resolved.

Table I. Peak positions and widths in the high angle diffraction data.

	$2\theta(\text{degrees})$	$\Delta\theta(\text{FWHM})$
Sample A	38.6	No preferred orientation
	40.6 Pt (111)	No preferred orientation
	42.1	Weak ordering
	47.3 Pt(002)	No preferred orientation
Sample B	30.5 Pt (n=-2)	2.5°
	35.5 Pt (n=-1)	3.0°
	38.2 Ag	1.2°
	40.6 Pt (n=0)	3.0°
	45.6 Pt (n=1)	4.5°
Sample C	30.5	Not measured
	35.5	2.3°
	38.2	1.3°
	40.54	2.5°
	45.7	4.0°
GaAs substrate (1 1 1)	27.3	.06°



XBL 924-567

Figure 1

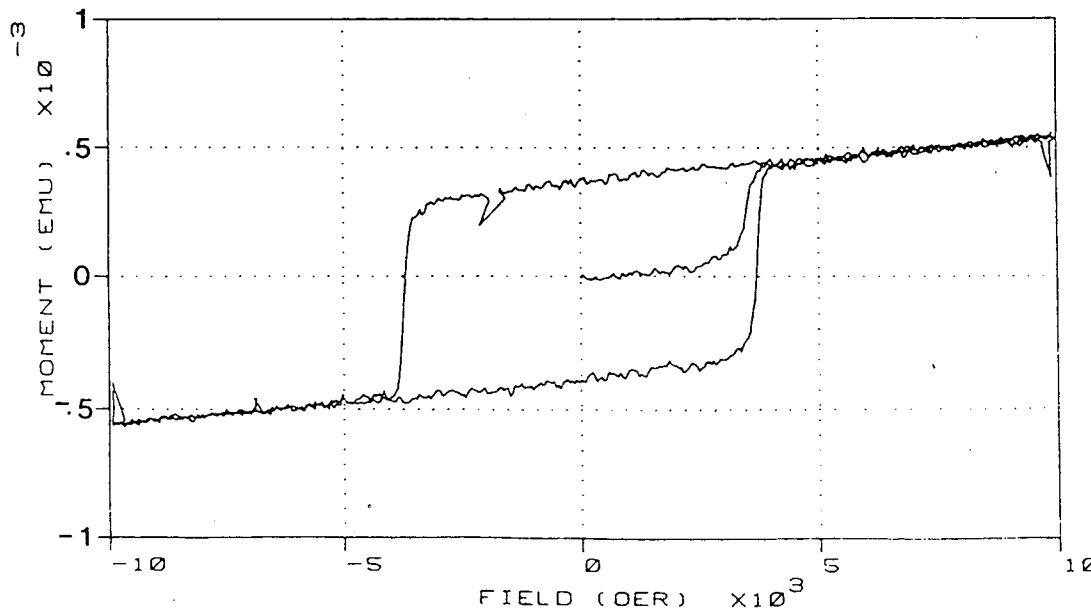
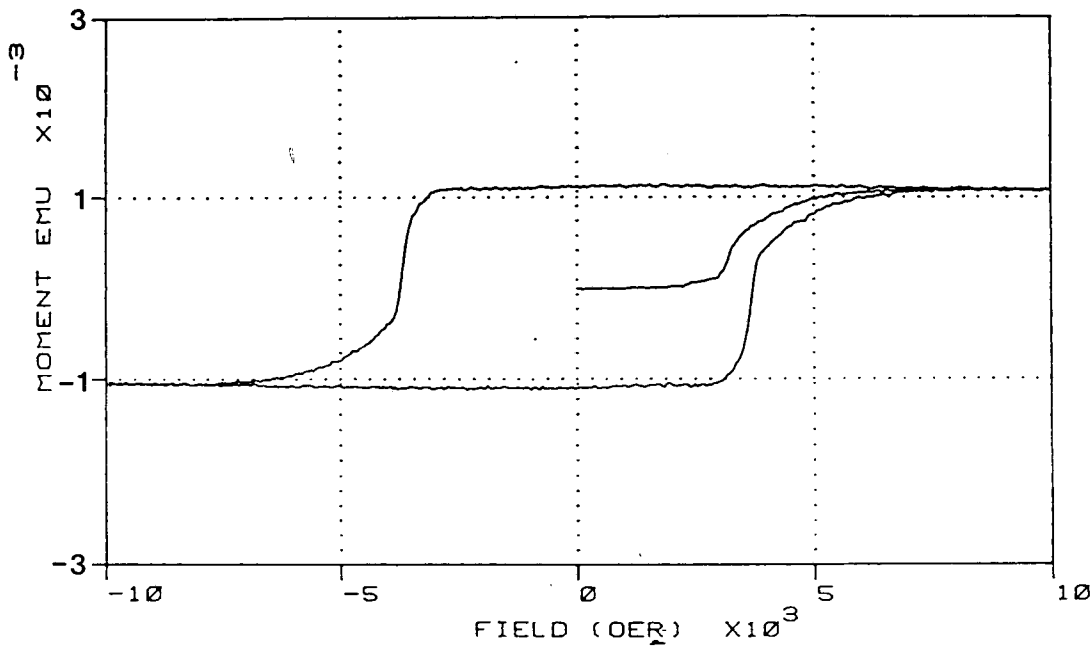
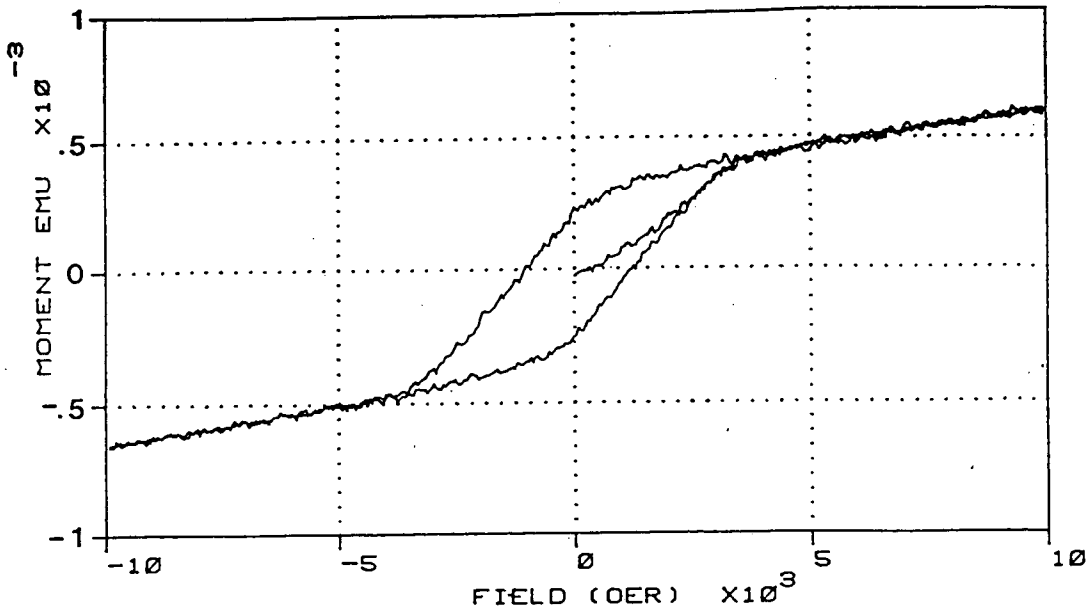
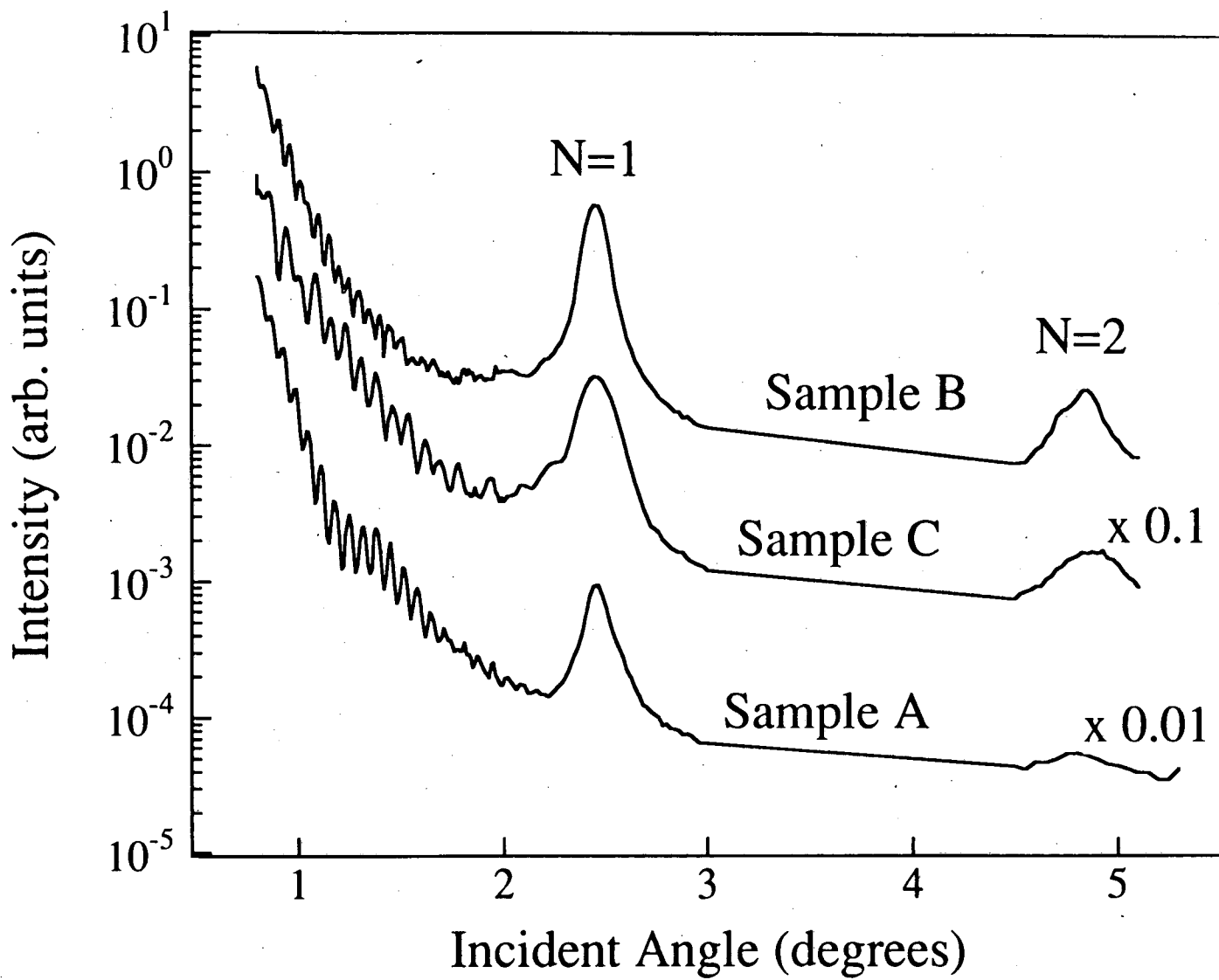
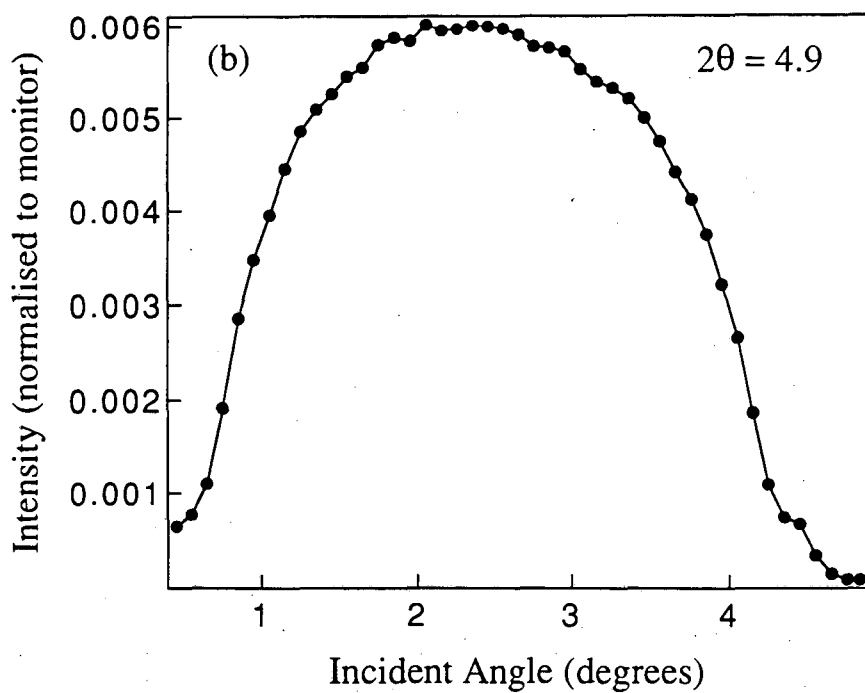
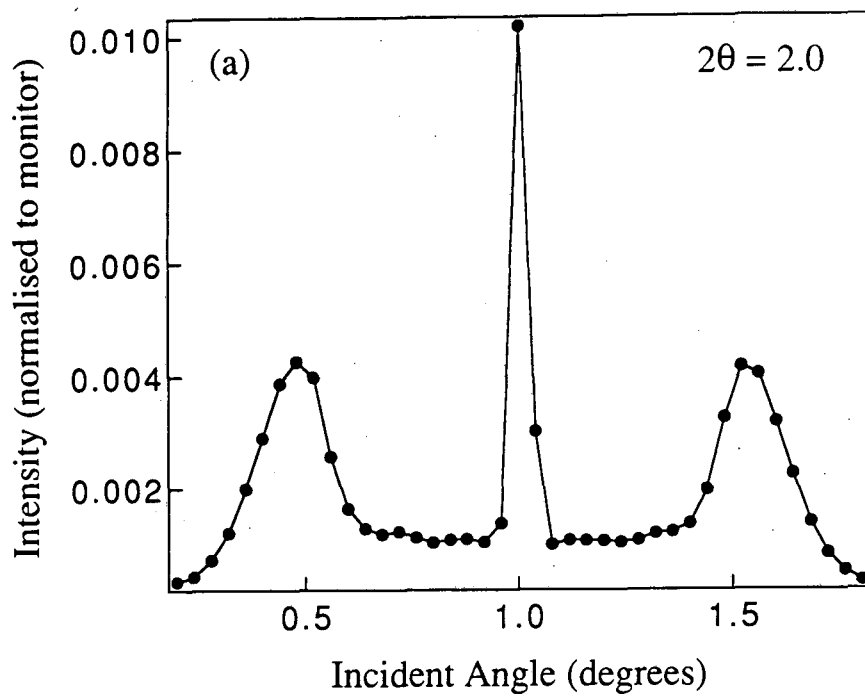


Figure 2



XBL 924-571

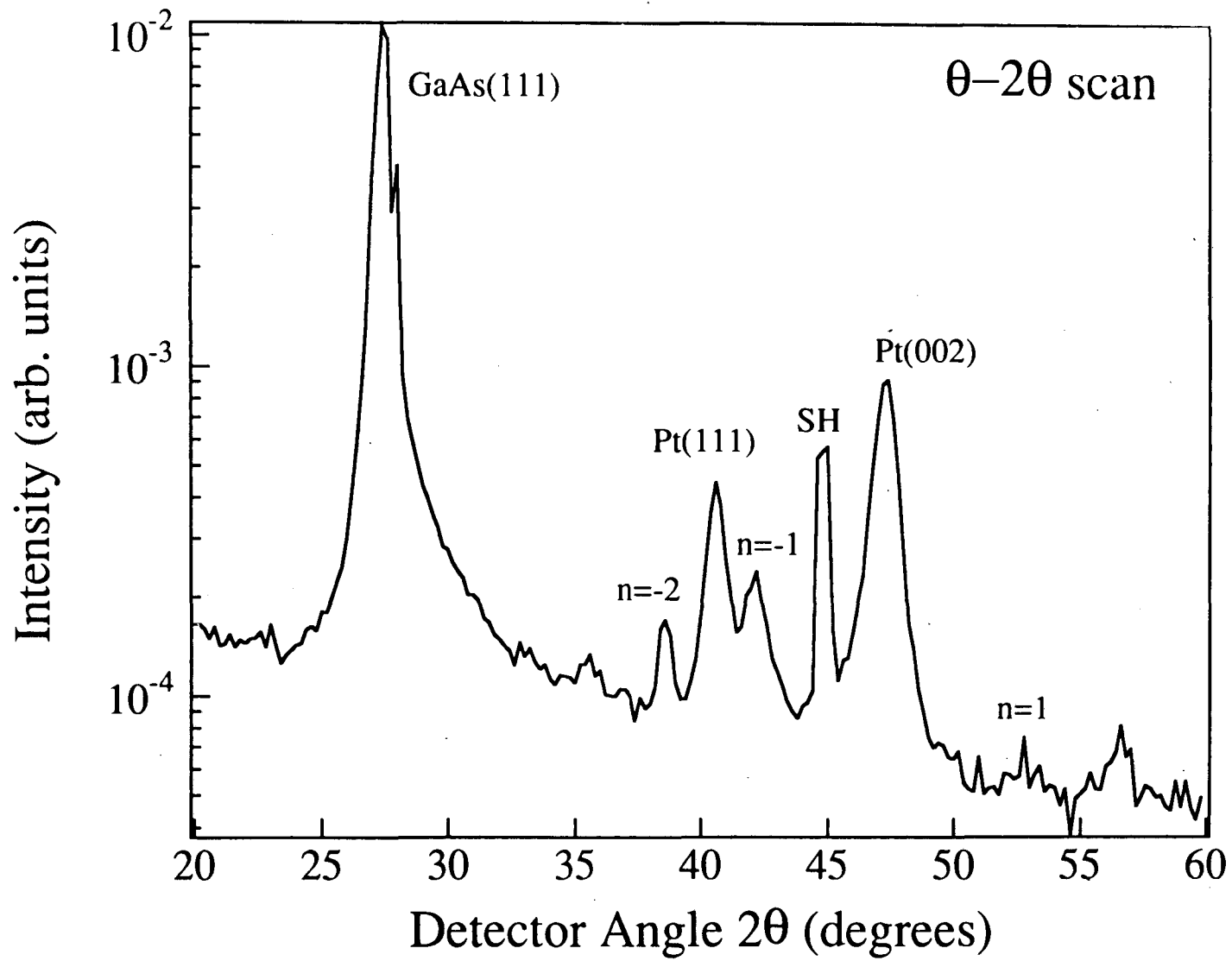
Figure 3



XBL 924-572

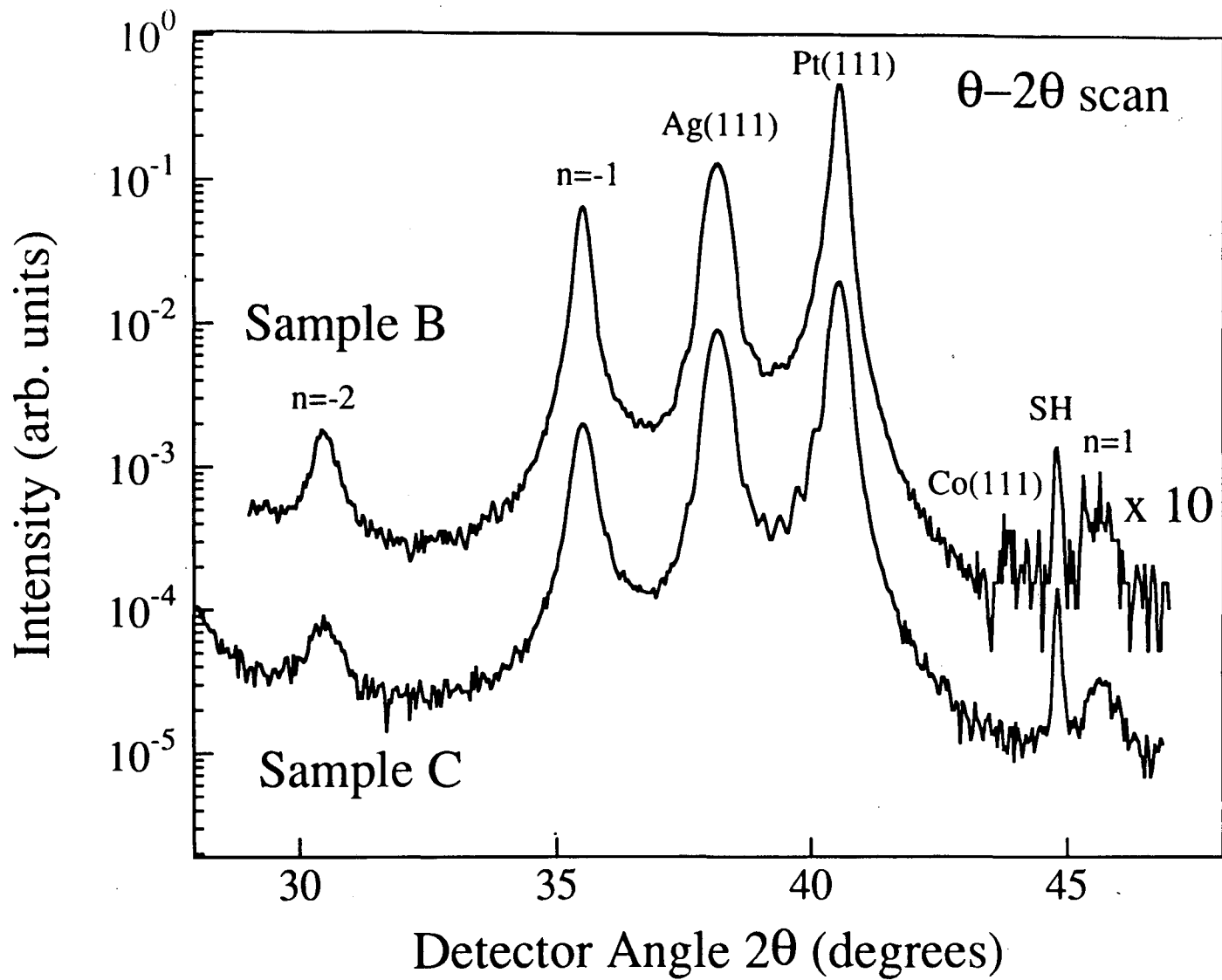
Figure 4

Figure 5

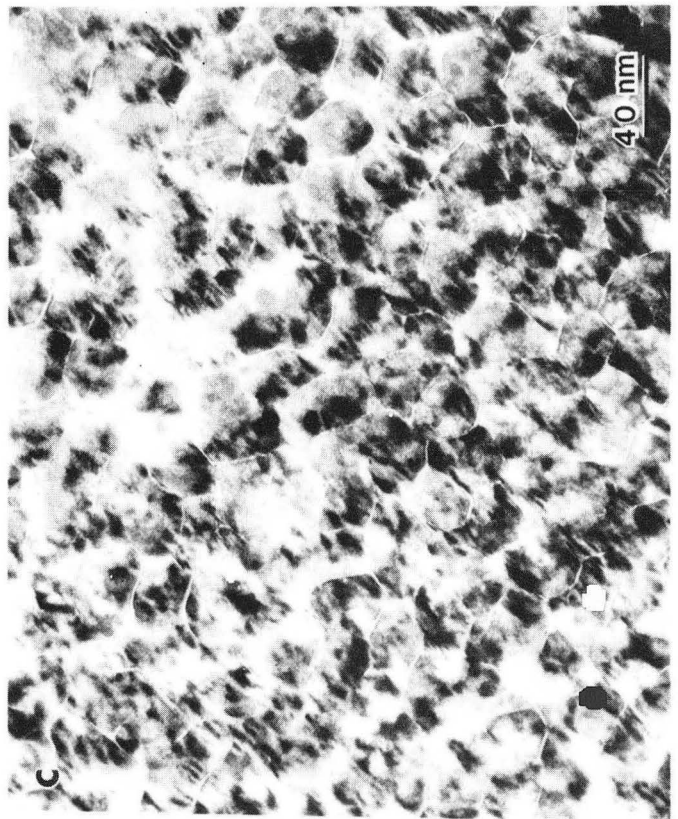
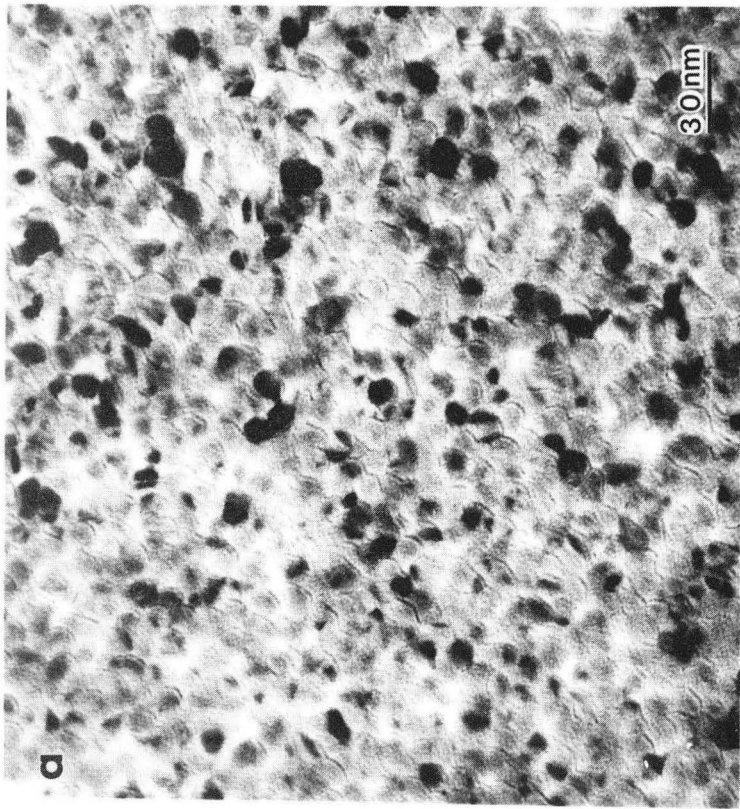
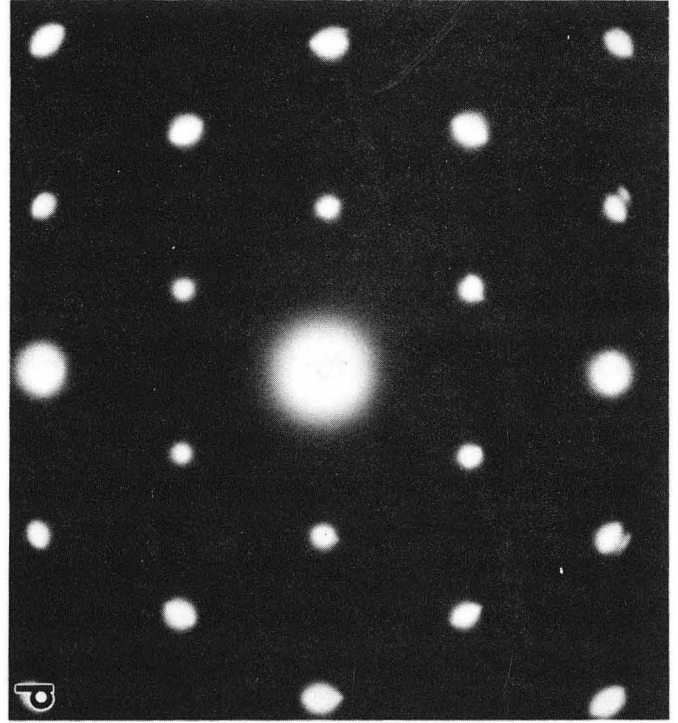
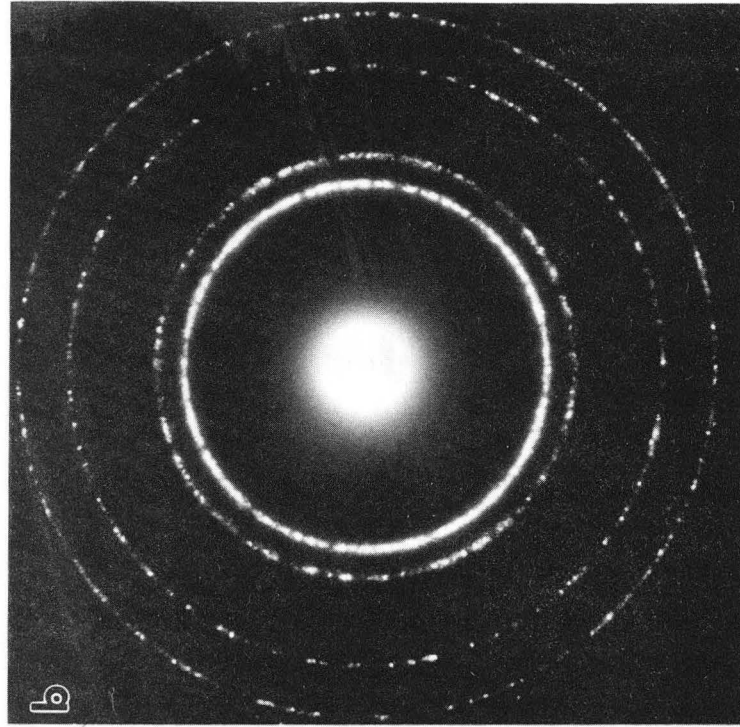


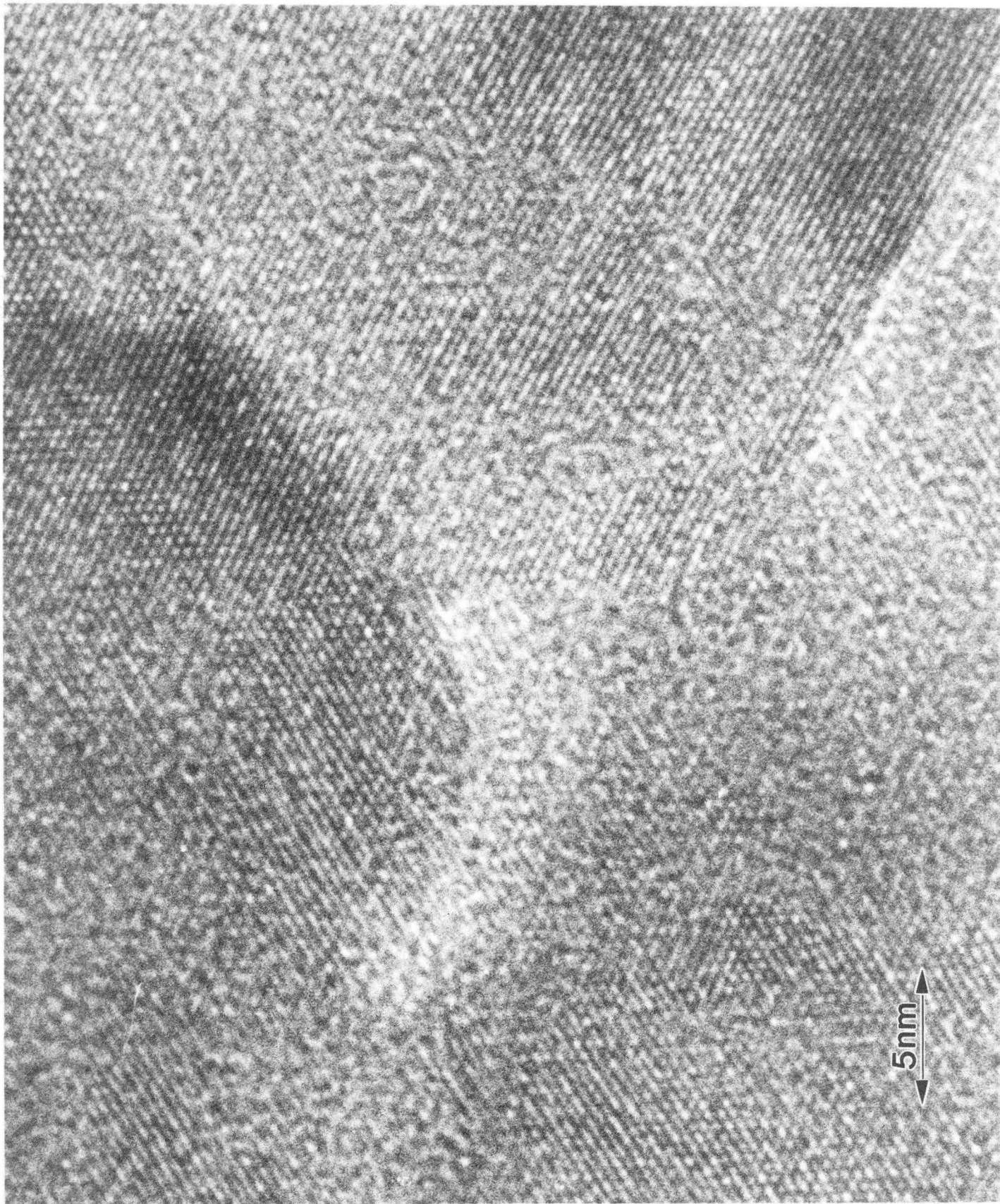
XBL 924-569

Figure 6



XBL 924-570





XBB 923-2162

Figure 8

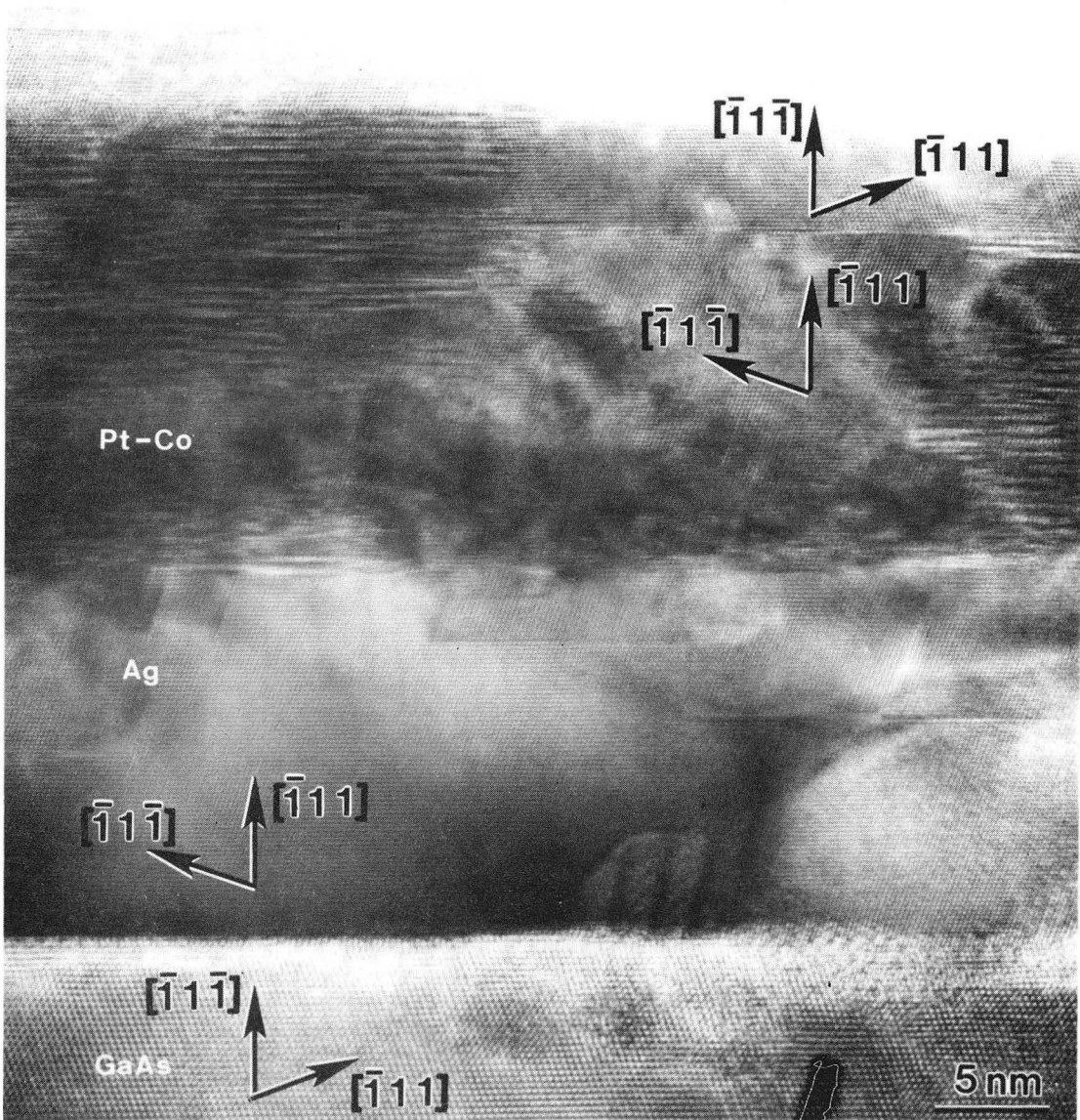
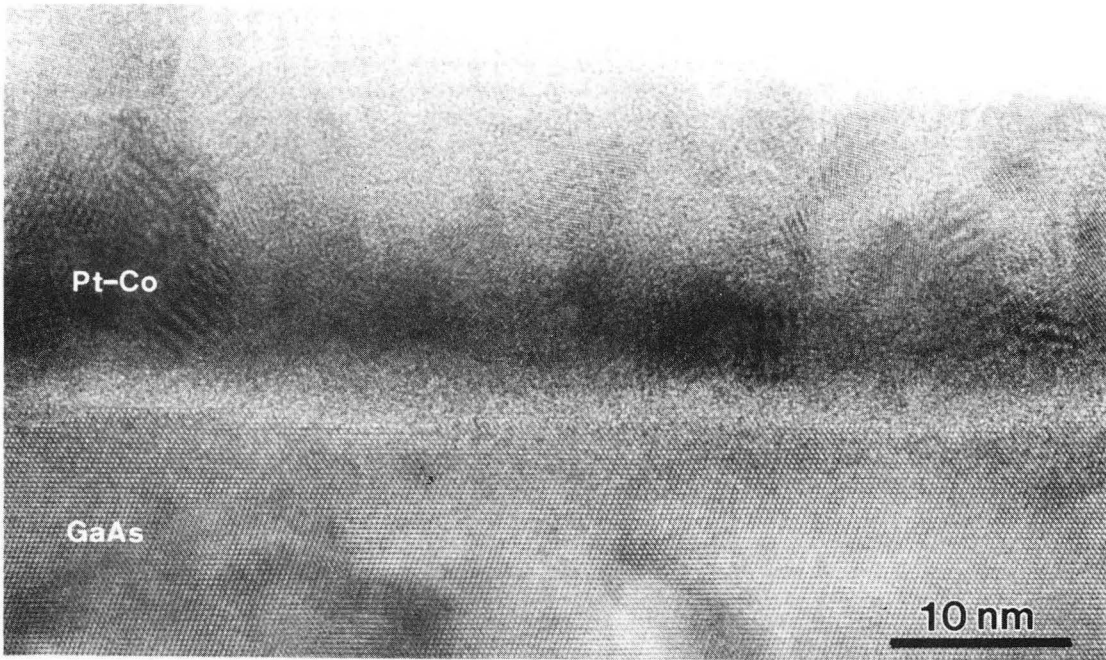


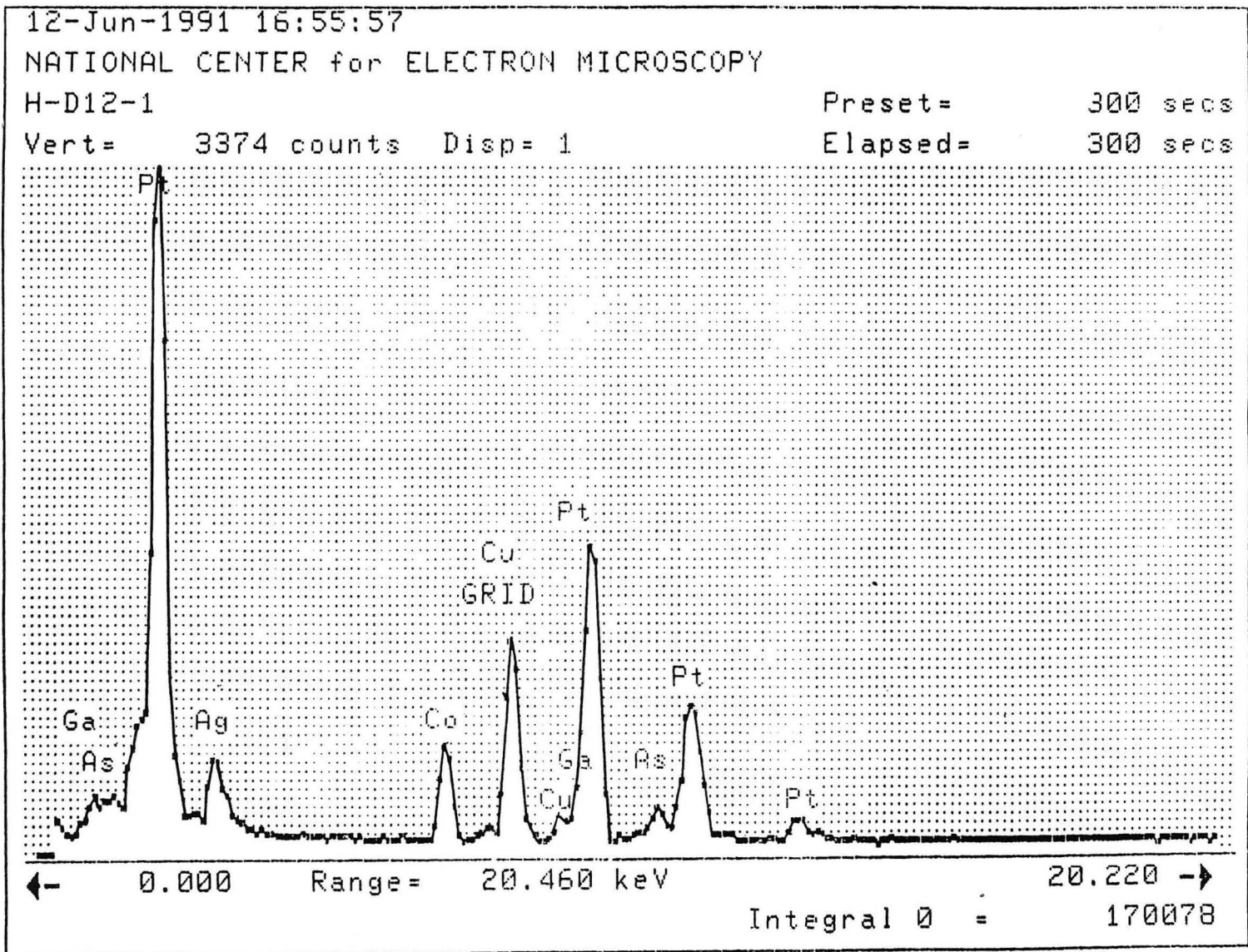
Figure 9

XBB 923-2163



XBB 917-5473A

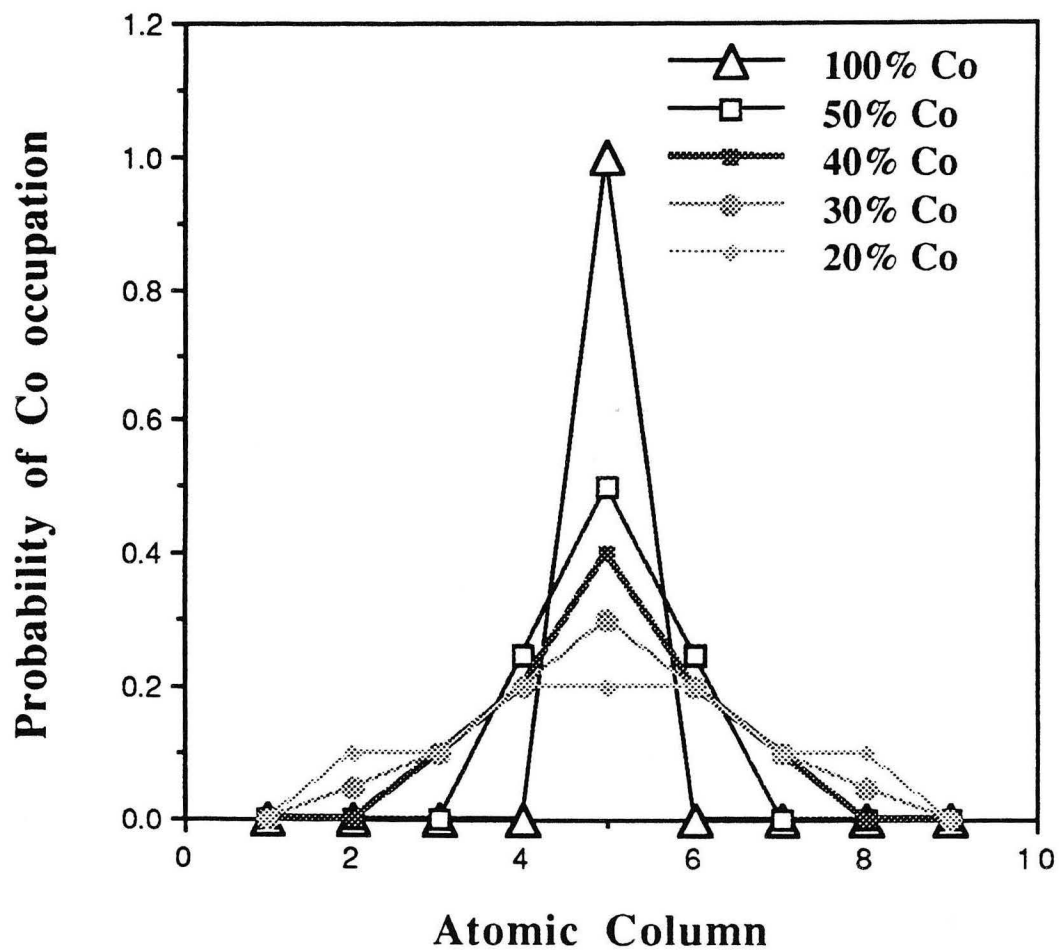
Figure 10



XBL 924-566

Figure 11

Models for Image simulation



XBL 924-568

Figure 12

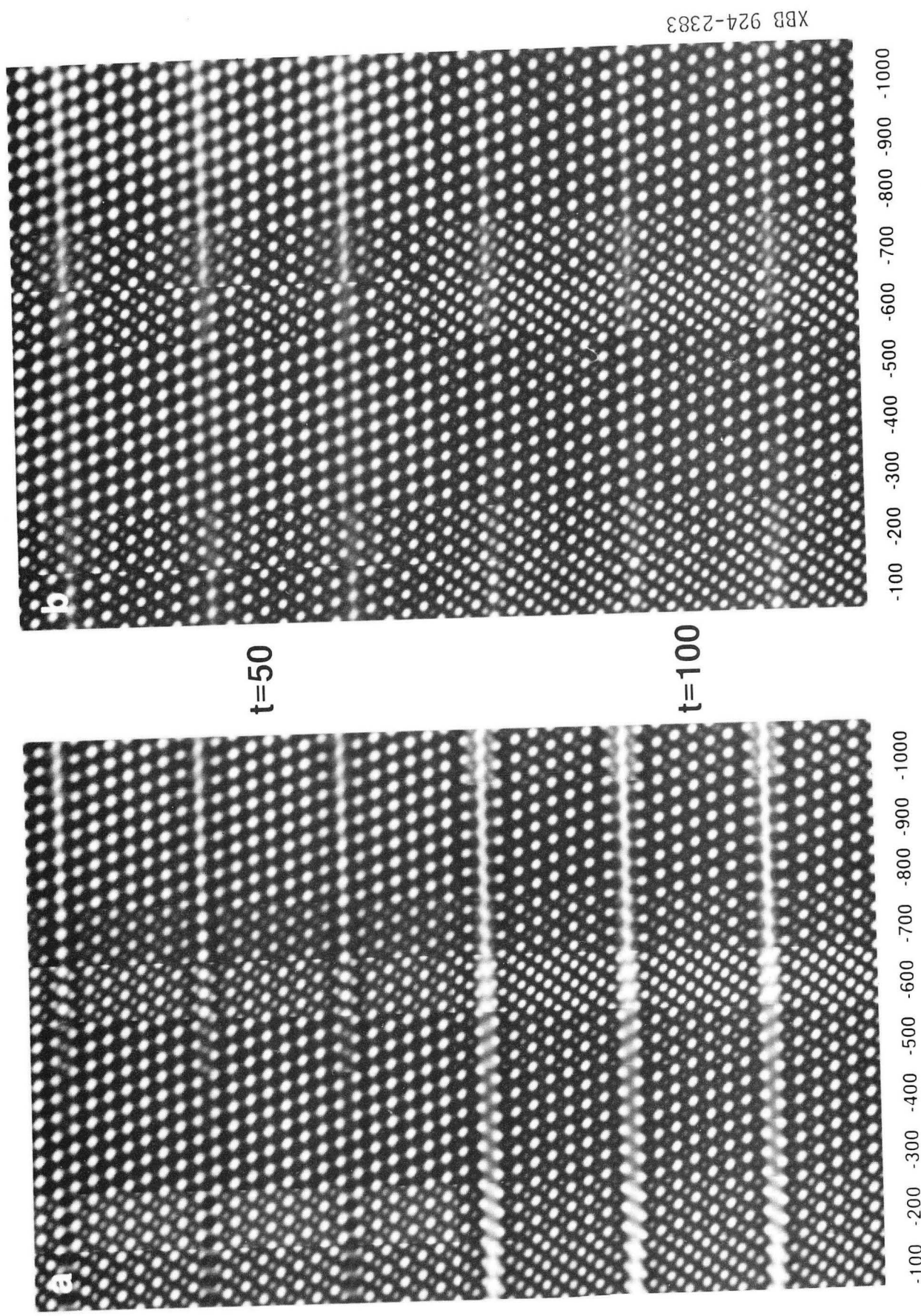


Figure 13

LAWRENCE BERKELEY LABORATORY
UNIVERSITY OF CALIFORNIA
TECHNICAL INFORMATION DEPARTMENT
BERKELEY, CALIFORNIA 94720